HIGH-FREQUENCY SONOCHEMICAL SYNTHESIS OF CHITOSAN-STABILISED SILVER NANOPARTICLES

Bożena Rokita[1,a,*], Renata Czechowska-Biskup[1,b,*], Malwina Olejniczak[1,c], Klaudia Jakubowska[1,d], Piotr Ulański[1,e]

[1] – Lodz University of Technology, Faculty of Chemistry, Institute of Applied Radiation Chemistry, Wroblewskiego 15 Str., 93-590 Lodz, Poland
[a] – ORCID: 0000-0002-9275-2175, [b] – ORCID: 0000-0001-8162-7670,
[c] – ORCID: 0009-0007-4292-5510, [d] – ORCID: 0009-0007-7756-0451,
[e] – ORCID: 0000-0002-4310-3574
**corresponding authors: bozena.rokita@p.lodz.pl, renata.czechowska-biskup@p.lodz.pl*

Abstract

Silver nanoparticles (AgNPs) stabilised by chitosan were synthesised via high-frequency ultrasound (620 kHz). The effects of pH (3–4) and the $AgNO_3$-to-chitosan molar ratio on nanoparticle formation, size, and colloidal stability were systematically evaluated. Acoustic cavitation generated highly reactive radical species, enabling efficient reduction of Ag^+ to Ag^0 without external reducing agents. UV-Vis spectroscopy confirmed nanoparticle formation, revealing surface plasmon resonance (SPR) bands at 405–410 nm (pH 3) and 420–425 nm (pH 4), indicating metal core diameters of 35–50 nm and pronounced pH-dependent structural variations. Dynamic light scattering showed hydrodynamic diameters of 100–250 nm. Notably, systems prepared at pH 3 exhibited a higher ζ-potential (~ +45 mV) and enhanced colloidal stability compared to those prepared at pH 4. These findings highlight high-frequency sonication as a clean and effective route for the additive-free synthesis of chitosan-stabilised AgNPs, with pH-driven polymer conformation playing a key role in controlling nanoparticle size and long-term stability.

Keywords: *silver nanoparticles, chitosan, additive-free reduction, sonochemical synthesis, high-frequency ultrasound*

Received: 30.03.2026
Accepted: 15.06.2026

1. Introduction

Silver nanoparticles (AgNPs) are widely investigated because their nanoscale dimensions give rise to physicochemical properties that differ markedly from those of bulk silver. A high surface-to-volume ratio and elevated surface free energy strongly influence thermodynamic stability and interfacial behaviour, while size-dependent electronic structure governs their optical response, manifested in the characteristic surface plasmon resonance (SPR) band observed in UV-Vis spectra [1–3]. However, the same high surface free energy renders metallic nuclei thermodynamically unstable with respect to aggregation. As a consequence, the physicochemical performance of AgNP dispersions is governed by the particle-size distribution, surface chemistry, and colloidal stability, making controlled nucleation and effective stabilisation essential during synthesis.

Conventional preparation of AgNPs relies predominantly on chemical reduction of silver salts using strong reducing agents, typically in the presence of additional stabilisers [4]. Although effective, such approaches introduce extra reagents and by-products that may complicate purification and affect the surface composition of the resulting nanoparticles. For this reason, increasing attention has been devoted to cleaner strategies, such as radiation- or light-induced synthesis [5–7], that minimise the use of chemical additives while maintaining control over particle formation.

Sonochemical synthesis represents one such alternative and is based on the physicochemical effects of high-intensity ultrasound in liquid media. When ultrasound propagates through an aqueous solution, acoustic cavitation occurs: microscopic bubbles form, grow, and collapse, generating localised extreme conditions. The fundamental principles of sonochemical nanomaterial synthesis and radical generation have been described previously [8]. The collapse of cavitation bubbles induces homolytic cleavage of water molecules, generating reactive $H^{\bullet}$ and $^{\bullet}OH$ radicals [8, 9]. While hydroxyl radicals are strongly oxidising, hydrogen radicals act as effective reducing agents, converting Ag^{+} to metallic Ag^{0}. This radical-mediated pathway enables silver ion reduction without the addition of external chemical reducing agents.

It has been demonstrated previously that ultrasound frequency influences the mechanism and yield of sonochemical reactions in aqueous media [10–13]. Most reported ultrasound-assisted nanoparticle syntheses employ low-frequency devices, typically probe systems operating at approximately 20 kHz or ultrasonic baths working at several tens of kilohertz. Low-frequency ultrasound (tens of kHz) promotes mechanochemical reactions, including polymer chain scission, while at medium and high frequencies (several hundred kHz), chemistry is dominated by the formation of water-derived free radicals ($H^{\bullet}$ and $^{\bullet}OH$). As a result, reaction outcomes observed at low frequencies cannot be directly extrapolated to systems operating in the several-hundred-kilohertz range. It has been shown that even at 360 kHz, some mechanochemical degradation still occurs in sonicated chitosan solutions [14, 15]. In this study, we aim to use $H^{\bullet}$ atoms, as well as chitosan-derived radicals formed by $^{\bullet}OH$ reactions with chitosan, to reduce silver ions, while avoiding excessive chitosan degradation. Hence, we decided to use high-frequency ultrasound (620 kHz).

Because newly generated silver nuclei possess high surface energy and readily aggregate, effective stabilisation is required. Chitosan, a cationic polysaccharide containing primary amino and hydroxyl groups, has been explored as a biocompatible stabiliser and surface-coating agent for AgNPs, where electrostatic interactions and polymer adsorption contribute to colloidal stabilisation [16–19]. In acidic media, protonated amino groups provide electrostatic repulsion, while adsorption of polymer chains onto the nanoparticle surface creates an additional steric barrier. Under

radical-generating conditions, chitosan may also contribute to the reduction of silver ions. The interesting properties of the resulting products also drive the interest in using chitosan as a stabiliser. Chitosan-stabilised Ag nanoparticles have been demonstrated in many studies to have efficient, broad-spectrum antibacterial [7, 17–25] and antifungal activity [5, 25], but low cytotoxicity to human skin cells [26, 27]. They have also been demonstrated to efficiently combat specific plant diseases, such as leaf fall disease on rubber trees caused by *Corynespora cassiicola* [28]. There are some preliminary indications of their anticancer activity against human lung adenocarcinoma cell lines [6].

The action of ultrasound on aqueous chitosan solutions induces partial polymer degradation through radical-mediated chain scission and mechanochemical effects [29, 30]. Changes in molecular weight and polymer conformation may alter the accessibility of functional groups and, consequently, the efficiency of nanoparticle stabilisation. As a polyelectrolyte, chitosan exhibits pH-dependent protonation-deprotonation equilibria, leading to conformational transitions that can significantly affect hydrodynamic particle dimensions and electrokinetic properties. Evaluation of ζ-potential and long-term stability is therefore particularly relevant in polymer-stabilised systems.

Although sonochemically synthesised chitosan-stabilised AgNPs have been reported before [31–33], the combined influence of pH, chitosan-to-silver molar ratio, and high-frequency ultrasonic treatment on nanoparticle size, electrokinetic properties, and long-term colloidal stability under additive-free conditions has not been systematically investigated.

Therefore, the aim of this study was to prepare chitosan-stabilised silver nanoparticles using a high-frequency sonication method (620 kHz) and to evaluate the effects of reaction pH and reagent molar ratio on nanoparticle formation, hydrodynamic size, ζ-potential, and stability over time in an additive-free system.

2. Materials and Methods

2.1. Materials and Preparation of $AgNO_3$-Chitosan Solutions

Medical-grade chitosan was obtained from Heppe Medical Chitosan GmbH (Germany). The chitosan employed in this study (designation 90/100) was characterised experimentally in our laboratory. The degree of deacetylation (DD) was determined by potentiometric titration according to [34] and was found to be 88%, while the viscosity-average molecular weight (Mv) was determined by viscometric measurements according to [35] and was 160 kDa. $AgNO_3$ (high purity grade) was purchased from Chempur (Poland). Sodium hydroxide solution (1 M NaOH, p.a.) was obtained from POCh (Poland), and acetic acid (80%) was supplied by Chemland (Poland). Argon (purity ≥ 99.9%) used for purging was provided by Linde Gas Poland. All reagents were used as received without further purification. High-purity water (0.055 μS cm^{-1}, TKA MicroPure system) was used throughout the study.

Aqueous chitosan solutions with concentrations of $1 \cdot 10^{-3}$ and $2 \cdot 10^{-3}$ mol/dm^3 (calculated with respect to glucosamine units bearing primary amino groups, corresponding to 0.161 and 0.322 g/dm^3, respectively) were prepared by dissolving the polymer in $5 \cdot 10^{-2}$ mol/dm^3 acetic acid and stirring for 24 h at room temperature to ensure complete dissolution. Subsequently, weighed amounts of silver nitrate were dissolved in chitosan solutions to achieve appropriate silver-ion concentrations. The compositions of the investigated systems are summarised in Table 1. The pH of the reaction mixture was adjusted using NaOH and monitored with a pH meter (Mettler Toledo SevenCompact

Duo, Switzerland). The instrument was calibrated using standard buffer solutions (pH 1.00, 7.00 and 10.00) supplied by Mettler Toledo.

Table 1. Composition of the $AgNO_3$-chitosan precursor aqueous solutions used for the AgNPs synthesis.

$AgNO_3$:chitosan molar ratio	$AgNO_3$ [mol/dm^3]	Chitosan [mol/dm^3]	Acetic acid [mol/dm^3]
1:2	$1 \cdot 10^{-3}$	$2 \cdot 10^{-3}$	$5 \cdot 10^{-2}$
2:2	$2 \cdot 10^{-3}$	$2 \cdot 10^{-3}$	$5 \cdot 10^{-2}$
2:1	$2 \cdot 10^{-3}$	$1 \cdot 10^{-3}$	$5 \cdot 10^{-2}$

The resulting precursor solutions were transferred into 10 cm^3 gas-tight glass ampoules (Figure 1a). Prior to sonochemical treatment, the samples were saturated with argon for 20 min to remove dissolved oxygen.

2.2. Sonochemical Synthesis of AgNPs

Silver nanoparticles were synthesised via high-frequency ultrasound reduction of Ag^+ in aqueous chitosan solutions (620.2 kHz). The reaction mixtures prepared as described in Section 2.1 were subjected to ultrasound under controlled conditions to induce radical-mediated reduction of silver ions.

Sonochemical experiments were performed using a URS-1000 ultrasonic reactor (Allied Signal Elac-Nautik, Kiel, Germany) consisting of a CESAR wave generator with amplifier, an ultrasonic transducer, and a thermostated cylindrical reactor with a capacity of 500 mL (see Figure 1b). The vibrating element of the transducer, covered with a stainless-steel plate, constituted the bottom of the reactor vessel. The reactor was filled with 500 mL of water, which served as an acoustic coupling medium. The reaction sample (10 mL) in a gas-tight, flat-bottom glass ampoule was positioned at a fixed location in the central region of the reactor. The water level in the reactor was maintained above the solution level in the ampoule to ensure efficient transmission of ultrasonic energy. Ultrasound was applied at a frequency of 620.2 kHz. The total power delivered to the system was 50 W, and the ultrasound dose rate was 74 W/kg (equivalent to 74 Gy/s), as determined by calorimetric dosimetry [12, 36]. Sonication was carried out for 60 min at a controlled temperature of 20 °C. The sonication time was selected based on preliminary experiments, which showed that the absorbance of the AgNP dispersion reached a maximum after approximately 60 min, while shorter sonication times resulted in incomplete reduction of Ag^+ ions, and longer treatment did not lead to significant further changes in the optical spectra.

2.3. Physicochemical Characterisation of AgNPs

2.3.1. UV-Vis Spectrophotometry

UV-Vis spectra of colloidal AgNP dispersions were recorded using a Shimadzu UV-2600 spectrophotometer in the wavelength range of 190–900 nm. Measurements were performed in quartz cuvettes with a 1 mm optical path length. Ultrapure water was used as a reference blank. All spectra were recorded 24 h after synthesis to ensure comparable measurement conditions and to allow stabilisation of the colloidal dispersion prior to optical analysis. For long-term stability studies, the AgNP dispersions were stored in sealed glass ampoules at 4 °C and protected from light. Samples were analysed after 1, 7, 14 and 30 days of storage.

2.3.2. Dynamic Light Scattering and ζ-Potential Measurements

Hydrodynamic diameter and ζ-potential of silver nanoparticles (AgNPs) were determined using a Zetasizer Nano ZS (Malvern Instruments Ltd.) equipped with a 633 nm He-Ne laser.

The hydrodynamic size was measured by dynamic light scattering (DLS) and calculated using cumulant analysis. Results are reported as the Z-average diameter. The polydispersity index (PDI), derived from the autocorrelation function, was used to quantify the width of the particle-size distribution. PDI values below 0.1 indicate a narrow size distribution, whereas higher values reflect increased polydispersity.

The ζ-potential, representing the electrokinetic potential at the slipping plane of nanoparticles dispersed in liquid, was determined by electrophoretic light scattering. Absolute ζ-potential values exceeding approximately 30 mV are generally considered indicative of electrostatically stabilised colloidal systems.

3. Results and Discussion

3.1. Sonochemical Formation of AgNPs and Optical Characterisation

The general mechanism of sonolysis of aqueous solutions is well known [11–13]. In brief, ultrasound waves of sufficient amplitude induce cavitation, i.e. the formation of small gas bubbles in the liquid. These bubbles oscillate with the ultrasound frequency. Their rapid, quasi-adiabatic collapse causes the gas to reach high temperatures, up to several thousand K, which in turn leads to thermal decomposition of water contained in the gas phase into H$^{\bullet}$ atoms and $^{\bullet}$OH radicals (Equation 1).

$$H_2O \rightarrow H^{\bullet} + {}^{\bullet}OH \quad (1)$$

Further effects of ultrasound on polymer include mechanochemical chain scission due to high gradients of liquid velocity in the vicinity of oscillating bubbles.

Sonochemically generated hydrogen atoms, being strongly reducing species, react with silver ions, yielding silver atoms (Equation 2). The latter coalesce to form silver nanoparticles (Equation 3), which become stabilised with chitosan.

$$H^{\bullet} + Ag^{+} \rightarrow H^{+} + Ag^{0} \quad (2)$$

$$n\ Ag^{0} \rightarrow (Ag)^{0}_{n} \quad (3)$$

It is estimated that the ratio of H$^{\bullet}$ to $^{\bullet}$OH escaping the bubbles is ca. 1:5 [13]. In the absence of other effects, this would make the reduction of silver ions ineffective, due to the prevailing oxidative character of the radical intermediates. However, $^{\bullet}$OH radicals react with both chitosan (k(4) = $6.4 \cdot 10^8$ dm^3/(mol·s) [15]) and acetic acid (k(5) = $1.6 \cdot 10^7$ dm^3/(mol·s) [37]) by hydrogen abstraction, yielding corresponding carbon-centred radicals of chitosan and acetic acid.

$$^{\bullet}OH + Chit \rightarrow H_2O + {}^{\bullet}Chit \quad (4)$$

$$^{\bullet}OH + H_3C\text{-}COOH \rightarrow H_2O + {}^{\bullet}H_2C\text{-}COOH \quad (5)$$

Considering the chitosan and acetic acid concentrations, as well as the rate constants of the above reactions (Equations 4 and 5), one can conclude that in our system, ca. 44–62% of $^{\bullet}$OH radicals react with chitosan, depending on the concentration of the latter.

Chitosan-derived radicals are mainly of the α-hydroxyalkyl type (for a detailed study on •OH reaction with chitosan, see [15]). Such radicals are known to possess reducing properties [38]. Therefore, they are expected to react with silver ions, causing their reduction.

$$\text{•Chit} + Ag^{+} \rightarrow \text{product} + Ag^{0} \quad (6)$$

Reaction of hydroxyl radicals with acetic acid (Equation 5) leads to α-carboxyalkyl radicals [39]. The latter have weaker reducing properties than α-hydroxyalkyl radicals [40, 41], therefore it is not clear if in the current case they also can reduce silver ions.

In this way, both kinds of primary radicals formed by cavitation, H• and •OH, contribute to the reduction of Ag^{+}.

In the context of the present work, it is of interest to estimate whether the radicals generated by 60 min of sonication are expected to reduce all silver ions initially present in the system. Since the ultrasound dose rate is 74 W/kg (74 Gy/s), the sonication time of 60 min corresponds to the total absorbed dose of ultrasound equal $2.7 \cdot 10^{5}$ J/kg (Gy). Our own measurements, on the apparatus and in the conditions used in this work, allow to estimate the total yield of H• and •OH radicals escaping the bubbles at ca. $1.2 \cdot 10^{-9}$ mol/J, which is in good accordance with values reported previously for similar conditions [11, 12]. Therefore, the total amount of these radicals formed during 60 min of sonication is ca. $3.2 \cdot 10^{-4}$ mol/dm^3, and this value should be the approximate amount of reduced silver ions. Since this amount is lower than the initial Ag^{+} concentration in our samples ($1–2 \cdot 10^{-3}$ mol/dm^3), it indicates that, very likely, some silver ions are still present in the system after sonication. This leaves room for some further post-reaction reduction of Ag^{+} to occur, which may be due to the mildly reducing properties of the chitosan itself [17, 21].

A question may be poised whether the structure and properties of chitosan itself change during our sonochemical processing. While it has been demonstrated that sonication does not significantly alter the degree of deacetylation of chitosan [42], a decrease in the average molecular weight is expected. It is known that chitosan, like many other polymers, undergoes degradation (chain scission) under ultrasound in solution [14, 43, 44]. It may be interesting to assess the final average molecular weight of chitosan at the end of our synthesis. While direct viscometric measurements cannot be made due to the presence of silver nanoparticles, this value can be estimated by calculation [45]. Taking into account a previous study conducted on aqueous solution of chitosan at the frequency of 360 kHz [14] and the general tendency of mechanochemical effects being less effective with increasing frequency [10–13], we expect that at the high frequency used in this work degradation will be mostly due to the scission of glycosidic bonds caused by the attack of •OH radicals [14, 15]. For the purpose of these calculations we assume that: (a) the sonochemical yield of •OH in our system is ca. $1.0 \cdot 10^{-9}$ mol/J, (b) in the absence of other •OH radical scavengers the sonochemical yield of degradation of chitosan is ca. 0.046 of the sonochemical yield of •OH [14], (c) in our case the fraction of •OH reacting with chitosan is 44–62% depending on the $AgNO_3$/chitosan ratio, (d) no other effects regarding chitosan take place, and (e) reaction given with Equation 6 does not influence the yield of degradation. Based on Eq. (3.28) in [45], we estimate that, in our experiments, the final average molecular weight of chitosan is in the range of 44 to 54 kDa. While this is a significant decrease from the starting point of 160 kDa, chitosan after the synthesis remains a long-chain polymer consisting of several hundred sugar units.

It should be noted, however, that other reactions may also occur in our system. For example, despite the high frequency of ultrasound application, we cannot rule out a mechanochemical effect of ultrasound on chitosan macromolecules. This can both

increase the number of chitosan radicals and further reduce the final molecular weight of chitosan beyond the effect caused by •OH radicals, thus modifying its stabilising properties.

The influence of pH and reagent ratio on the sonochemical formation of silver nanoparticles in the $AgNO_3$-chitosan system was evaluated based on optical characterisation. A schematic overview of the reaction system and the polymer-mediated stabilisation of the forming nanoparticles is presented in Figure 1.

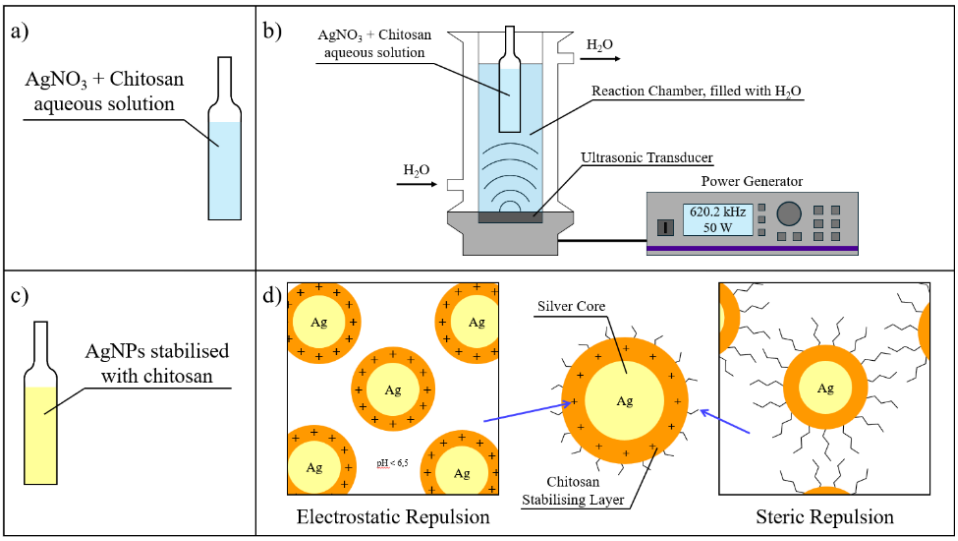

Figure 1. Schematic overview of the high-frequency ultrasonic reactor system and the stepwise formation of chitosan-stabilised AgNPs: (a) precursor $AgNO_3$-chitosan solution, (b) placement of the reaction ampoule in the ultrasonic reactor (620.2 kHz), (c) generation of colloidal AgNPs after sonochemical treatment, (d) proposed electrosteric stabilisation mechanism involving surface-associated chitosan chains and pH-dependent protonated amino groups generating electrostatic repulsion and steric protection.

During sonication, the initially colourless solutions developed a yellow colouration, indicating the formation of nanosized silver. UV-Vis spectra recorded after the reaction are shown in Figure 2. All samples exhibited a characteristic absorption band in the range of 380–450 nm, attributed to the surface plasmon resonance (SPR) of spherical AgNPs [3, 46].

The position and intensity of the SPR band depended on both pH and the molar ratio of $AgNO_3$-to-chitosan. At pH 3, the plasmon maximum was observed at 405–410 nm. Increasing the pH to 4 resulted in a red shift of the SPR band toward 420–425 nm. Within a given pH series, the position of the SPR maximum changed only slightly with the $AgNO_3$ chitosan molar ratio, indicating that pH was the dominant factor affecting the spectral shift, whereas composition mainly influenced the absorbance intensity. Such a shift is commonly associated with an increase in particle size, partial aggregation, or changes in the dielectric environment surrounding the metallic core [3, 47, 48]. In addition, broader spectral profiles were observed at pH 4, suggesting a wider particle size distribution.

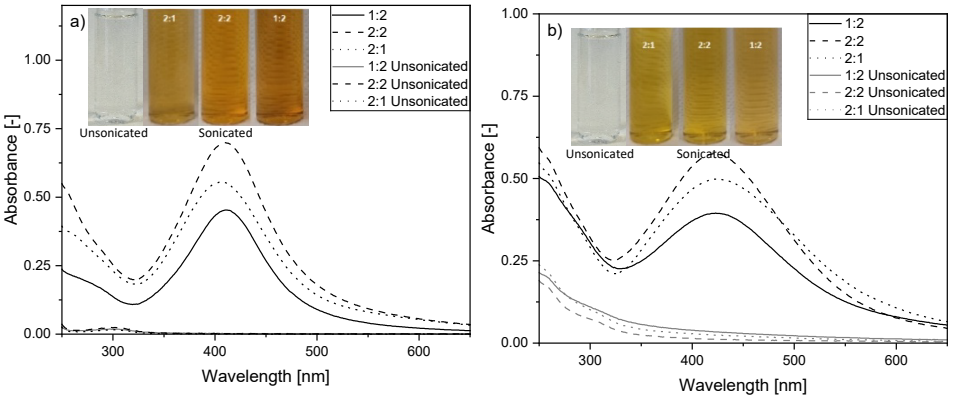

Figure 2. UV-Vis absorption spectra of colloidal AgNPs obtained after 60 min of sonication at 620.2 kHz (P = 50 W, T = 20 °C) for different $AgNO_3$-chitosan molar ratios at (a) pH 3 and (b) pH 4. Spectra were recorded 24 h after synthesis.

A systematic dependence of the SPR band intensity on the $AgNO_3$-to-chitosan molar ratio was also observed. At both pH 3 and pH 4, the highest absorbance was observed for the equimolar system (2:2), followed by 2:1, whereas the lowest absorbance was observed for the 1:2 ratio. The higher absorbance observed in systems with higher relative concentrations of Ag^+ indicates a greater number of plasmonic species formed during sonochemical reduction. Conversely, an excess of chitosan relative to Ag^+ may limit effective nucleation or result in smaller metallic cores with lower extinction intensity. The evolution of absorbance during storage and the long-term stability of the obtained dispersions are discussed in Section 3.3.

Macroscopic observations were consistent with the spectroscopic data. Samples prepared at pH 4 exhibited a darker yellow colouration than those prepared at pH 3, consistent with red-shifted SPR bands. The more intense colouration at pH 4 may reflect larger effective particle sizes or subtle interparticle interactions affecting the optical response.

The observed SPR positions are consistent with the literature, where spherical AgNPs typically exhibit plasmonic maxima in the range of 400–420 nm [3, 22, 48, 49]. For example, Chen *et al.* [49] reported AgNPs with a plasmon maximum at approximately 410 nm and a metallic core size of ~25 nm. According to the analytical model proposed by Car and Krstulović [48], which correlates SPR wavelength with the size distribution of colloidal silver nanoparticles, a plasmon maximum at approximately 410 nm corresponds to AgNP core diameters of about 35–40 nm, whereas a red-shift toward ~420–425 nm indicates somewhat larger particles, typically around 45–50 nm. Thus, the SPR maxima observed in the present study (~410 nm at pH 3 and ~422 nm at pH 4) suggest that nanoparticles formed at higher pH possess slightly larger metallic cores. Variations in pH are known to influence nanoparticle nucleation and growth kinetics as well as the interfacial environment, thereby affecting the optical properties of the colloidal system [3].

The differences between systems prepared at pH 3 and 4 can be rationalised by considering the role of chitosan in nanoparticle stabilisation. At lower pH, protonation of amino groups enhances electrostatic repulsion and promotes more extended polymer conformations, facilitating effective surface coverage of the forming nanoparticles. At slightly higher pH, reduced protonation decreases electrostatic stabilisation, which may

contribute to larger effective particle sizes or broader size distributions, as suggested by the spectral features.

3.2. Hydrodynamic Size Distribution and ζ-Potential of AgNP Dispersion

To further elucidate the influence of pH and reagent ratio on nanoparticle size and colloidal stability, hydrodynamic diameter and ζ-potential were determined by dynamic light scattering. The results are summarised in Table 2. To maintain consistency with the UV-Vis measurements, the DLS analyses were performed 24 h after synthesis to allow stabilisation of the colloidal system following sonication and to avoid short-term post-sonication changes in particle-size distribution.

It is important to emphasise that DLS provides the hydrodynamic diameter, which reflects not only the metallic core but also the surrounding polymer layer and the solvation shell. Therefore, the relatively large Z-average values reported here (~98–257 nm) represent the effective size of polymer-coated nanoparticles dispersed in solution rather than the metallic core diameter alone.

Table 2. Hydrodynamic diameter (Z-average), polydispersity index (PDI), and ζ-potential of AgNP dispersions synthesised by high-frequency sonication. Measurements were performed 24 h after synthesis.

pH	$AgNO_3$:chitosan molar ratio	Hydrodynamic diameter [nm]	PDI [-]	ζ-potential [mV]
3	1:2	257 ± 21	0.428 ± 0.013	42.1 ± 9.9
	2:2	211 ± 8	0.655 ± 0.053	46.4 ± 8.3
	2:1	186 ± 10	0.382 ± 0.009	47.2 ± 0.8
4	1:2	98 ± 7	0.216 ± 0.032	32.0 ± 7.0
	2:2	167 ± 6	0.219 ± 0.001	38.3 ± 3.6
	2:1	186 ± 9	0.248 ± 0.009	25.5 ± 7.9

A clear dependence of hydrodynamic size on pH was observed. At pH 3, the Z-average diameters ranged from 186 ± 10 nm to 257 ± 21 nm, depending on the $AgNO_3$-chitosan ratio. In contrast, at pH 4, smaller hydrodynamic sizes were generally recorded, particularly for the $1 \cdot 10^{-3}$ mol/dm^3 $AgNO_3$: $2 \cdot 10^{-3}$ mol/dm^3 chitosan system (98 ± 7 nm). Under equimolar conditions (2:2), the hydrodynamic diameter decreased from 211 ± 8 nm at pH 3 to 167 ± 6 nm at pH 4. These findings indicate that pH significantly affects the effective particle dimensions in dispersion. The larger hydrodynamic diameters observed at pH 3 are likely related to the extended conformation of protonated chitosan chains. At pH 4, partial deprotonation promotes a more compact polymer structure, resulting in smaller hydrodynamic diameters.

The polydispersity index (PDI) values ranged from 0.216 to 0.655. Systems prepared at pH 4 exhibited lower PDI values (0.216–0.248), indicating narrower size distributions compared to selected systems at pH 3, where higher PDI values (up to 0.655) suggest broader distributions. The relatively high PDI value observed for the 2:2 system at pH 3 (0.655) suggests the coexistence of differently sized particle populations, possibly reflecting simultaneous nucleation and growth processes under these conditions.

ζ-potential measurements further confirmed the role of electrostatic stabilisation. At pH 3, ζ-potential values were consistently high (approximately +42 to +47 mV), indicating strong electrostatic repulsion and good colloidal stability. At pH 4, ζ-potential values decreased to +25 to +38 mV, reflecting reduced surface charge density due to

partial deprotonation of amino groups. The lowest ζ-potential value (+25.5 ± 7.9 mV) was observed for the $2 \cdot 10^{-3}$ mol/dm^3 $AgNO_3$: $1 \cdot 10^{-3}$ mol/dm^3 chitosan system, suggesting comparatively weaker electrostatic stabilisation under these conditions.

Literature data indicate that sonochemically prepared chitosan-stabilised AgNP dispersions may exhibit hydrodynamic sizes ranging from several tens to approximately one hundred nanometers, depending strongly on synthesis conditions and formulation parameters [31]. For example, concentrated aqueous dispersions of silver-chitosan nanoparticles prepared under ultrasonic conditions were reported to contain populations around 60–100 nm, demonstrating stable polymer-nanoparticle interactions [31]. Other ultrasound-assisted systems employing different reductants or stabilisers have also produced nanoparticles with effective sizes in the tens of nanometers [32]. General reviews on ultrasound-assisted fabrication of polysaccharide-coated nanostructures further highlight the influence of polymer molecular weight, concentration, and sonication parameters on the resulting size distribution [33]. The somewhat larger hydrodynamic dimensions observed in the present study may therefore arise from the relatively high molecular weight of chitosan used and its extended conformation under acidic conditions, which increases the apparent particle size measured by DLS.

While UV-Vis spectrophotometry predominantly reflects the plasmonic response of the metallic core, DLS provides the hydrodynamic diameter, including the polymer shell and solvation layer. The combined optical and colloidal analyses thus provide complementary information on nanoparticle structure and stability.

3.3. Long-term Stability of Chitosan-AgNPs

The long-term colloidal stability of the prepared AgNP dispersions was evaluated by monitoring UV-Vis spectra for up to 30 days after synthesis (Figures 3 and 4). Changes in the intensity, position, and shape of the surface plasmon resonance (SPR) band were analysed as indicators of nanoparticle growth, aggregation, or structural rearrangement within the polymer-metal system. Changes in hydrodynamic diameter, polydispersity index (PDI), ζ-potential and pH during storage for systems prepared at pH 3 are summarised in Table 3.

For the system with $AgNO_3$:chitosan ratio 1:2 (Figure 3a), the SPR band remained nearly unchanged for at least 30 days. No significant shift in the maximum wavelength and no noticeable band broadening were observed, indicating a stable metallic core size and preserved colloidal integrity. DLS measurements performed after 30 days showed hydrodynamic diameters of approximately 186–214 nm (Table 3), while the ζ-potential remained above +40 mV. This suggests that the observed variations in hydrodynamic size are relatively small and may result from gradual polymer rearrangement or weak clustering rather than from extensive nanoparticle aggregation. In the 2:1 system (Figure 3b), a gradual decrease in SPR intensity was detected. After approximately 30 days, the absorbance decreased by about 18% relative to the initial value. Importantly, this decrease was not accompanied by a red shift of the SPR maximum. After 30 days, the hydrodynamic diameter remained within the range of 245–277 nm during storage (Table 3), while the ζ-potential values remained above +40 mV. The persistence of high positive surface charge indicates that electrostatic stabilisation is largely maintained, and the decrease in absorbance likely reflects partial sedimentation of larger clusters or redistribution of particles within the dispersion rather than irreversible core coalescence. For the equimolar 2:2 system (Figure 3c), the SPR intensity remained stable during the first 7 days and subsequently increased, reaching an absorbance approximately 30% higher than the initial value after prolonged storage. The absence of band broadening suggests controlled structural evolution rather than uncontrolled growth.

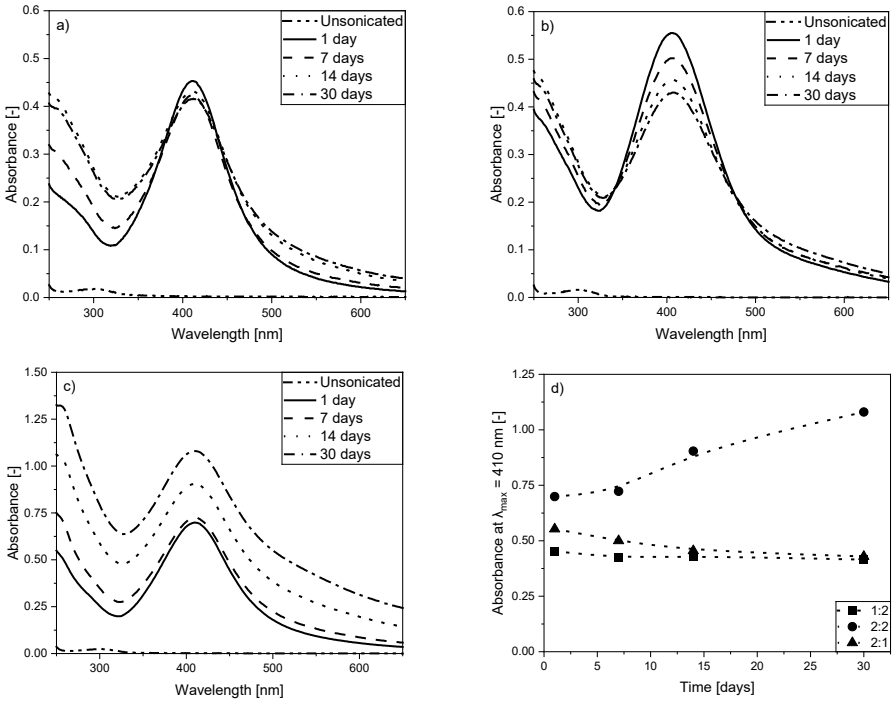

Figure 3. Time-dependent changes in the UV-Vis spectra of AgNP dispersions at pH 3 for different $AgNO_3$:chitosan molar ratios: (a) 1:2; (b) 2:1; (c) 2:2; (d) absorbance at the SPR maximum plotted as a function of time.

Table 3. Hydrodynamic diameter (Z-average), polydispersity index (PDI), ζ-potential, and pH of chitosan-stabilised AgNP dispersions synthesised by high-frequency sonication at pH 3.

$AgNO_3$:Ch molar ratio	Time [day]	pH	Hydrodynamic diameter [nm]	PDI	ζ-potential [mV]
2:1	1	2.95 ± 0.01	257 ± 21	0.428 ± 0.013	42.1 ± 9.9
	7	3.15 ± 0.01	250 ± 1	0.379 ± 0.053	41.4 ± 5.8
	14	3.10 ± 0.02	277 ± 45	0.347 ± 0.030	45.5 ± 0.3
	30	3.14 ± 0.01	245 ± 32	0.350 ± 0.035	42.8 ± 5.1
2:2	1	3.16 ± 0.05	211 ± 8	0.655 ± 0.053	46.4 ± 6,3
	7	3.17 ± 0.02	232 ± 4	0.503 ± 0.058	46.5 ± 4.2
	14	3.02 ± 0.02	275 ± 26	0.355 ± 0.002	48.0 ± 0.6
	30	3.16 ± 0.04	237 ± 31	0.298 ± 0.018	45.9 ± 5.2
1:2	1	2.95 ± 0.01	186 ± 10	0.382 ± 0.009	47.2 ± 0.8
	7	3.05 ± 0.01	197 ± 5	0.367 ± 0.046	46.4 ± 0.7
	14	3.01 ± 0.02	214 ± 22	0.374 ± 0.022	43.6 ± 0.1
	30	3.05 ± 0.02	206 ± 9	0.311 ± 0.004	44.5 ± 5.3

Consistently, the hydrodynamic diameter after 30 days remained within the range of approximately 211–275 nm (Table 3), with ζ-potential still exceeding +40 mV. This supports the interpretation that the observed optical changes may be associated with the gradual completion of reduction processes or the reorganisation of initially formed silver clusters within the stabilising chitosan matrix.

An increase in absorbance was observed between the 1st and 7th day for all investigated systems, indicating continued structural evolution of the dispersion after sonication, which may be attributed to completion of reduction processes or reorganisation of initially formed silver clusters within the chitosan matrix. The systems prepared at pH 4 showed slightly more pronounced time-dependent changes compared to those at pH 3, although no rapid destabilisation was observed. For the 1:2 ratio (Figure 4a), the absorbance decreased within the first 7 days and subsequently stabilised. According to the DLS measurements (Table 4), the hydrodynamic diameter remained in the range of approximately 160–175 nm over the investigated period, while ζ-potential values were around +30 mV. The reduced surface charge relative to pH 3 suggests weaker electrostatic repulsion and increased susceptibility to interparticle interactions. In the 2:1 system (Figure 4b), the decrease in SPR intensity was more gradual and approximately linear over time. The hydrodynamic diameter varied between approximately 211–248 nm during storage (Table 4), while the ζ-potential decreased from about +41 mV after synthesis to almost +33 mV after several days. The lower surface charge magnitude at pH 4 than at pH 3 likely facilitates progressive aggregation or sedimentation, explaining the continuous decrease in optical density. For the 2:2 system (Figure 4c), behaviour similar to Figure 4a was observed, with an initial decrease in absorbance followed by stabilisation. The hydrodynamic diameter after storage remained in the range of approximately 189–211 nm (Table 4), again accompanied by ζ-potential values around +30 mV. These results indicate that although complete destabilisation does not occur, the colloidal systems at pH 4 exhibit slightly weaker electrostatic stabilisation than those prepared at pH 3.

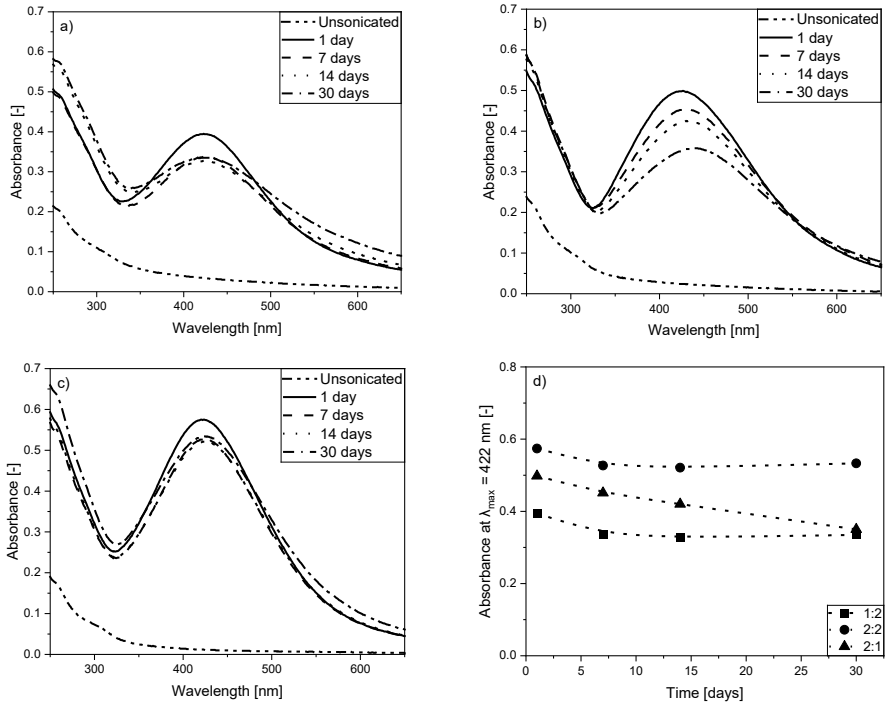

Figure 4. Time-dependent changes in the UV-Vis spectra of AgNP dispersions at pH 4 for different AgNO3:chitosan molar ratios: (a) 1:2; (b) 2:1; (c) 2:2; (d) absorbance at the SPR maximum plotted as a function of time.

Table 4. Hydrodynamic diameter (Z-average), polydispersity index (PDI), ζ-potential, and pH of chitosan-stabilised AgNP dispersions synthesised by high-frequency sonication at pH 4.

$AgNO_3$:Ch molar ratio	Time [day]	pH	Hydrodynamic diameter [nm]	PDI	ζ-potential [mV]
2:1	1	4.10 ± 0.01	211 ± 18	0.205 ± 0.022	41.2 ± 2.1
	7	4.09 ± 0.01	248 ± 14	0.215 ± 0.019	33.2 ± 6.6
	14	4.07 ± 0.01	238 ± 3	0.199 ± 0.012	31.0 ± 7.6
	30	4.06 ± 0.02	240 ± 15	0.235 ± 0.046	36.4 ± 5.9
2:2	1	4.03 ± 0.06	189 ± 15	0.233 ± 0.014	30.0 ± 4.9
	7	4.06 ± 0.02	195 ± 8	0.235 ± 0.007	29.9 ± 3.8
	14	4.02 ± 0.03	211 ± 27	0.290 ± 0.053	34.2 ± 2.5
	30	4.05 ± 0.02	207 ± 3	0.273 ± 0.005	31.4 ± 4.6
1:2	1	3.96 ± 0.01	160 ± 9	0.248 ± 0.009	25.5 ± 7.9
	7	4.03 ± 0.01	175 ± 4	0.254 ± 0.028	31.6 ± 0.1
	14	3.97 ± 0.01	173 ± 11	0.256 ± 0.005	35.5 ± 4.3
	30	4.02 ± 0.01	171 ± 7	0.248 ± 0.004	32.5 ± 0.3

The stabilisation mechanism in the present system can be described as electrosteric stabilisation, arising from the combined effects of electrostatic repulsion (from the protonated amino groups of chitosan) and steric hindrance provided by adsorbed polymer chains. At pH 3, a higher degree of protonation enhances chain expansion and surface charge density, leading to ζ-potential values above +40 mV and improved long-term stability.

At pH 4, partial deprotonation reduces the surface charge to approximately +30 mV, weakening electrostatic contributions and allowing particles to approach more closely. However, the hydrodynamic diameters remain relatively constant over time (Tables 3 and 4), suggesting that the observed optical changes are primarily attributable to limited clustering or structural rearrangements rather than uncontrolled aggregation.

Chitosan may also undergo slow structural modification in acidic aqueous environments. Gradual degradation, driven by acid-catalysed hydrolysis or conformational changes, may influence both DLS measurements and optical response independently of metallic core transformations. Therefore, some of the temporal evolution observed in UV-Vis spectra may be associated with time-dependent polymer rearrangement.

Literature reports indicate that the long-term stability of chitosan-stabilised AgNPs strongly depends on polymer molecular weight, degree of protonation, and sonication conditions [31–33]. Systems with sufficiently high surface charge and adequate steric protection have been shown to maintain dispersion stability for extended periods [19, 31]. In contrast to the commonly used low-frequency ultrasound systems (~20–40 kHz), higher ultrasound frequencies favour chemical effects of cavitation and enhanced generation of reactive radicals, while reducing the contribution of purely mechanical effects such as intense polymer chain scission. Such conditions may provide more controlled reduction processes and improved stability of polymer-stabilised nanoparticle dispersions.

The present results demonstrate that high-frequency sonochemical synthesis, combined with chitosan stabilisation, can yield dispersions that exhibit sustained electrosteric stabilisation, particularly under acidic conditions. Such stability is

advantageous for applications requiring prolonged storage, including antimicrobial coatings, wound dressings, and biomedical formulations.

Overall, the combined UV-Vis, DLS, and ζ-potential analyses indicate that AgNP dispersions prepared at pH 3 exhibit superior long-term stability compared to those obtained at pH 4, with stability governed primarily by polymer protonation and the resulting electrosteric interactions.

Taken together, the results suggest that the long-term stability of the AgNP dispersions is largely governed by the protonation state of chitosan, which determines the magnitude of electrostatic repulsion and the effectiveness of electrosteric stabilisation.

4. Conclusions

Silver nanoparticles stabilised by chitosan can be successfully synthesised using high-frequency ultrasound (620.2 kHz) without the addition of external chemical reducing agents. Formation of AgNPs is confirmed by the appearance of a characteristic SPR band in the range of 405–425 nm, whose position and intensity are strongly dependent on pH and reagent ratio.

Optical analysis reveals that increasing pH from 3 to 4 induces a red shift of the SPR band and broader spectral profiles, suggesting changes in particle-size distribution and the dielectric environment. The $AgNO_3$-to-chitosan molar ratio significantly influences nanoparticle formation efficiency, with the equimolar system exhibiting the highest plasmon intensity.

Dynamic light scattering measurements demonstrate that the hydrodynamic diameter of the nanoparticles is governed primarily by polymer conformation rather than metallic core size. At pH 3, extended protonated chitosan chains lead to larger effective hydrodynamic sizes (186–257 nm) and high ζ-potential values (> +40 mV), indicating strong electrostatic stabilisation. At pH 4, partial deprotonation results in a reduced ζ-potential (~ +30 mV) and increased susceptibility to time-dependent structural changes.

Long-term stability studies confirm that dispersions prepared at pH 3 exhibit superior colloidal stability over at least 30 days, maintaining stable SPR profiles and high surface charge. Systems prepared at pH 4 show moderate decreases in optical density over time, consistent with reduced electrostatic repulsion and limited clustering. The combined UV-Vis, DLS, and ζ-potential analyses indicate that electrosteric stabilisation provided by chitosan plays a key role in controlling nanoparticle size and long-term dispersion stability.

Due to their high colloidal stability, particularly at pH 3, the obtained chitosan-stabilised AgNP dispersions may find applications not only in antimicrobial materials but also in wound dressings, biomedical coatings, and dermatological formulations, where long-term colloidal stability is essential [50–54].

Overall, the results demonstrate that high-frequency sonochemical synthesis in the presence of chitosan provides a clean and effective route to stable AgNP dispersions, with physicochemical properties tunable through pH and reagent ratio. A limitation of the present study is the lack of direct microscopic characterisation of the synthesised nanoparticles. Although UV-Vis spectroscopy, DLS measurements, and ζ-potential analysis provided consistent evidence of nanoparticle formation and colloidal stability, future studies including TEM or SEM analyses would enable direct verification of nanoparticle morphology, core size distribution, and aggregation state.

5. Acknowledgements

This article was completed while Malwina Olejniczak was a Doctoral Candidate in the Interdisciplinary Doctoral School at the Lodz University of Technology, Poland.

6. Author Contributions

Conceptualisation, B.R. and R.C.-B.; methodology, B.R. and R.C.-B.; validation, B.R., R.C.-B.; and P.U.; formal analysis, B.R., R.C.-B., P.U., M.O., and K.J.; investigation, B.R., R.C.-B., M.O., and K.J.; resources, B.R., R.C.-B., and P.U.; data curation, B.R., R.C.-B., and M.O.; writing-original draft preparation, B.R., R.C.-B., P.U., and M.O.; writing-review and editing, B.R., R.C.-B., P.U., and M.O.; visualisation, B.R., R.C.-B., and M.O.; supervision, B.R. and R.C.-B.; project administration, B.R. and R.C.-B.; funding acquisition, B.R., R.C.-B., and P.U. All authors have read and agreed to the published version of the manuscript.

7. References

[1] Duman H, Eker F, Akdaşçi E, Witkowska AM, Bechelany M, Karav S; (2024) Silver nanoparticles: A comprehensive review of synthesis methods and chemical and physical properties. Nanomaterials 14(18), 1527. **DOI:** 10.3390/nano14181527

[2] Hosny S, Gaber GA, Ragab MS, Ragheb MA, Anter M, Mohamed LZ; (2026) A comprehensive review of silver nanoparticles (AgNPs): synthesis strategies, toxicity concerns, biomedical applications, AI-driven advancements, challenges, and future perspectives. Arabian Journal for Science and Engineering 51, 13667–13714. **DOI:** 10.1007/s13369-025-10612-0

[3] Yadav S, Vohra N; (2024) A comprehensive review of silver nanoparticles: classification, synthesis, properties, applications, and toxicity. PEXACY International Journal of Pharmaceutical Science 3(12), 25–51. **DOI:** 10.5281/zenodo.14567901

[4] Zheng H, Li Y, Li W, Zhou S, Huang C, Du L; (2024) Ultrasound induced biosynthesis of silver nanoparticles embedded into chitosan polymers: Investigation of its anti-cutaneous squamous cell carcinoma effects. Open Chemistry 22(1), 20240018. **DOI:** 10.1515/chem-2024-0018

[5] Jannoo K, Teerapatsakul C, Punyanut A, Pasanphan W; (2015) Electron beam assisted synthesis of silver nanoparticle in chitosan stabilizer: Preparation, stability and inhibition of building fungi studies. Radiation Physics and Chemistry 112(5), 177–188. **DOI:** 10.1016/j.radphyschem.2015.03.035

[6] Devendrapandi G, Padmanaban D, Thanikasalam R, Panneerselvam A, Palraj R, Rajabathar JR, Rajendiran N, Balu R, Oh TH, Ramasundaram S; (2023) Direct sunlight induced room temperature synthesis of anticancer and catalytic silver nanoparticles by shrimp shell waste derived chitosan. International Journal of Biological Macromolecules 252, 126205. **DOI:** 10.1016/j.ijbiomac.2023.126205

[7] Huang NM, Radiman S, Lim HN, Khiew PS, Chiu WS, Lee KH, Syahida A, Hashim R, Chia CH; (2009) γ-Ray assisted synthesis of silver nanoparticles in chitosan solution and the antibacterial properties. Chemical Engineering Journal 155(1–2), 499–507. **DOI:** 10.1016/j.cej.2009.07.040

[8] Xu H, Zeiger BW, Suslick KS; (2013) Sonochemical synthesis of nanomaterials. Chemical Society Reviews 42(7), 2555–2567. **DOI:** 10.1039/C2CS35282F

[9] Ashokkumar M; (2011) The characterization of acoustic cavitation bubbles – An overview. Ultrasonics Sonochemistry 18(4), 864–872. **DOI:** 10.1016/j.ultsonch. 2010.11.016

[10] Brotchie A, Grieser F, Ashokkumar M; (2010) Characterization of acoustic cavitation bubbles in different sound fields. The Journal of Physical Chemistry B 114(34), 11010–11016. **DOI:** 10.1021/jp105618q

[11] Von Sonntag C, Mark G, Tauber A, Schuchmann H–P; (1999) OH radical formation and dosimetry in the sonolysis of aqueous solutions. In: Mason TJ (ed.), Advances in Sonochemistry, JAI Press, vol. 5, pp. 109–145. ISBN: 9780762303311, eBook.

[12] Tauber A; (1998) Mechanistische Untersuchungen zur Sonolyse organischer Verbindungen in wäßriger Lösung. Doctoral dissertation, Bochum University, Mülheim an der Ruhr

[13] Mark G, Tauber A, Laupert R, Schuchmann H–P, Schulz D, Mues A, von Sonntag C; (1998) OH-radical formation by ultrasound in aqueous solution-Part II: Terephthalate and Fricke dosimetry and the influence of various conditions on the sonolytic yield. Ultrasonics Sonochemistry 5, 41–52. **DOI:** 10.1016/S1350-4177(98)00012-1

[14] Czechowska-Biskup R, Rokita B, Lotfy S, Ulanski P, Rosiak JM; (2005) Degradation of chitosan and starch by 360-kHz ultrasound. Carbohydrate Polymers 60(2), 175–184. **DOI:** 10.1016/j.carbpol.2004.12.001

[15] Ulanski P, von Sonntag C; (2000) OH-Radical-induced chain scission of chitosan in the absence and presence of dioxygen. Journal of the Chemical Society, Perkin Transactions 2 2000, 2022–2028. **DOI:** 10.1039/b003952g

[16] Mulvaney P; (1996) Surface plasmon spectroscopy of nanosized metal particles. Langmuir 12(3), 788–800. **DOI:** 10.1021/la9502711

[17] Wei D, Sun W, Qian W, Ye Y, Ma X; (2009) The synthesis of chitosan-based silver nanoparticles and their antibacterial activity. Carbohydrate Research 344(17), 2375–2382. **DOI:** 10.1016/j.carres.2009.09.001

[18] Tran HV, Tran LD, Ba CT, Vu HD, Nguyen TN, Pham DG, Nguyen PX; (2010) Synthesis, characterization, antibacterial and antiproliferative activities of monodisperse chitosan- based silver nanoparticles. Colloids and Surfaces A: Physicochemical and Engineering Aspects 360(1–3), 32–40. **DOI:** 10.1016/ j.colsurfa.2010.02.007

[19] Venkatesham M, Ayodhya D, Madhusudhan A, Veera Babu N, Veerabhadram G; (2014) A novel green one-step synthesis of silver nanoparticles using chitosan: catalytic activity and antimicrobial studies. Applied Nanoscience 4(1), 113–119. **DOI:** 10.1007/s13204-012-0180-y

[20] Paulkumar K, Gnanajobitha G, Vanaja M, Pavunraj M, Annadurai G; (2017) Green synthesis of silver nanoparticle and silver based chitosan bionanocomposite using stem extract of Saccharum officinarum and assessment of its antibacterial activity. Advances in Natural Sciences: Nanoscience and Nanotechnology 8(3), 035019. **DOI:** 10.1088/2043-6254/aa7232

[21] Wongpreecha J, Polpanich D, Suteewong T, Kaewsaneha C, Tangboriboonrat P; (2018) One-pot, large-scale green synthesis of silver nanoparticles-chitosan with enhanced antibacterial activity and low cytotoxicity. Carbohydrate Polymers 199, 641–648. **DOI:** 10.1016/j.carbpol.2018.07.039

[22] Chen J, Fan L, Yang C, Wang S, Zhang M, Xu J, Luo S; (2020) Facile synthesis of Ag nanoparticles-loaded chitosan antibacterial nanocomposite and its application

in polypropylene. International Journal of Biological Macromolecules 161, 1286–1295. **DOI:** 10.1016/j.ijbiomac.2020.07.151

[23] Mirda E, Idroes R, Khairan K, Tallei TE, Ramli M, Earlia N, Maulana A, Idroes GM, Muslem M, Jalil Z; (2021) Synthesis of chitosan-silver nanoparticle composite spheres and their antimicrobial activities. Polymers 13(22), 3990. **DOI:** 10.3390/polym13223990

[24] Ge J, Li M, Fan J, Celia C, Xie Y, Chang Q, Deng X; (2024) Synthesis, characterization, and antibacterial activity of chitosan-chelated silver nanoparticles. Journal of Biomaterials Science, Polymer Edition 35(1), 45–62. **DOI:** 10.1080/09205063.2023.2265629

[25] Biao L, Tan S, Wang Y, Guo X, Fu Y, Xu F, Zu Y, Liu Z; (2017) Synthesis, characterization and antibacterial study on the chitosan-functionalized Ag nanoparticles. Materials Science and Engineering: C 76, 73–80. **DOI:** 10.1016/j.msec.2017.02.154

[26] Dara PK, Mahadevan R, Digita PA, Visnuvinayagam S, Kumar LRG, Mathew S, Ravishankar CN, Anandan R; (2020) Synthesis and biochemical characterization of silver nanoparticles grafted chitosan (Chi-Ag-NPs): in vitro studies on antioxidant and antibacterial applications. SN Applied Sciences 2(4), 665. **DOI:** 10.1007/s42452-020-2261-y

[27] Aljohani MM, Abu-Rayyan A, Elsayed NH, Alatawi FA, Al-Anazi M, Mustafa SK, Albalawi RK, Abdelmonem R; (2023) One-pot microwave synthesis of chitosan-stabilized silver nanoparticles entrapped polyethylene oxide nanofibers, with their intrinsic antibacterial and antioxidant potency for wound healing. International Journal of Biological Macromolecules 235, 123704. **DOI:** 10.1016/j.ijbiomac.2023.123704

[28] Nhien LTA, Luong ND, Tien LTT, Luan LQ; (2018) Radiation synthesis of silver nanoparticles/chitosan for controlling leaf fall disease on rubber trees causing by Corynespora cassiicola. Journal of Nanomaterials 2018, 1–9. **DOI:** 10.1155/2018/7121549

[29] Caruso RA, Ashokkumar M, Grieser F; (2002) Sonochemical formation of gold sols. Langmuir 18(21), 7831–7836. **DOI:** 10.1021/la020276f

[30] Remita H, Remita S; (2010) Metal clusters and nanomaterials: contribution of radiation chemistry. In: Wishart JF, Rao BSM (eds.), Recent Trends in Radiation Chemistry, World Scientific, pp. 347–383. **DOI:** 10.1142/9789814282093_0013

[31] Francesko A, Cano Fossas M, Petkova P, Fernandes MM, Mendoza E, Tzanov T; (2017) Sonochemical synthesis and stabilization of concentrated antimicrobial silver-chitosan nanoparticle dispersions. Journal of Applied Polymer Science 134(30), 45136. **DOI:** 10.1002/app.45136

[32] Guzmán K, Kumar B, Vallejo MJ, Grijalva M, Debut A, Cumbal L; (2019) Ultrasound-assisted synthesis and antibacterial activity of gallic acid-chitosan modified silver nanoparticles. Progress in Organic Coatings 129, 229–235. **DOI:** 10.1016/j.porgcoat.2019.01.009

[33] Bera S, Mondal D; (2019) A role for ultrasound in the fabrication of carbohydrate-supported nanomaterials. Journal of Ultrasound 22(2), 131–156. **DOI:** 10.1007/s40477-019-00363-8

[34] Czechowska-Biskup R, Jarosińska D, Rokita B, Ulański P, Rosiak JM; (2012) Determination of degree of deacetylation of chitosan - Comparison of methods. Progress on Chemistry and Application of Chitin and its Derivatives 17, 5–20.

[35] Czechowska-Biskup R, Wach RA, Rosiak JM, Ulański P; (2018) Procedure for determination of the molecular weight of chitosan by viscometry. Progress on Chemistry and Application of Chitin and its Derivatives 23, 45–54. **DOI:** 10.15259/PCACD.23.04

[36] Hallez L, Touyeras F, Hihn JY, Klima J; (2007) Energetic balance in an ultrasonic reactor using focused or flat high frequency transducers. Ultrasonics Sonochemistry 14(6), 739–749. **DOI:** 10.1016/j.ultsonch.2006.12.012

[37] Buxton GV, Greenstock CL, Helman WP, Ross AB; (1988) Critical review of rate constants for reactions of hydrated electrons, hydrogen atoms and hydroxyl radicals ($^{\cdot}OH/^{\cdot}O^{-}$) in aqueous solution. Journal of Physical and Chemical Reference Data 17(2), 513–886. **DOI:** 10.1063/1.555805

[38] Ulanski P, Bothe E, Rosiak JM, von Sonntag C; (1994) OH-radical-induced crosslinking and strand breakage of poly(vinyl alcohol) in aqueous solution in the absence and presence of oxygen. A pulse radiolysis and product study. Macromolecular Chemistry and Physics 195(4), 1443–1461. **DOI:** 10.1002/macp.1994.021950427

[39] Neta P, Simic M, Hayon E; (1969) Pulse radiolysis of aliphatic acids in aqueous solutions. I. Simple monocarboxylic acids. Journal of Physical Chemistry 73(12), 4207–4213. **DOI:** 10.1021/j100846a029

[40] Ulanski P, Bothe E, Rosiak JM, von Sonntag C; (1996) Radiolysis of the poly(acrylic acid) model 2,4-dimethylglutaric acid: a pulse radiolysis and product study. Journal of the Chemical Society, Perkin Transactions 2 1996, 5–12. **DOI:** 10.1039/p29960000005

[41] Ulanski P, Bothe E, Hildenbrand K, Rosiak JM, von Sonntag C; (1996) Hydroxyl-radical-induced reactions of poly(acrylic acid); a pulse radiolysis, EPR and product study. Part I. Deoxygenated aqueous solutions. Journal of the Chemical Society, Perkin Transactions 2 1996, 13–22. **DOI:** 10.1039/p29960000013

[42] Tang ESK, Huang M, Lim LY; (2003) Ultrasonication of chitosan and chitosan nanoparticles. International Journal of Pharmaceutics 265(1–2), 103–114. **DOI:** 10.1016/S0378-5173(03)00408-3

[43] Mason TJ, Lorimer PJ; (2002) Applied sonochemistry: the uses of power ultrasound in chemistry and processing, Wiley-VCH. **DOI:** 10.1002/352760054X

[44] Rokita B, Czechowska-Biskup R, Ulanski P, Rosiak JM; (2005) Modification of polymers by ultrasound treatment in aqueous solution. e-Polymers 5(1), 024. **DOI:** 10.1515/epoly.2005.5.1.261

[45] Coqueret X, Sabharwal S, Khairul Zaman HMD, Czechowska-Biskup R, Wach RA, Rosiak JM, Ulanski P, Gulrez SKH, Al-Assaf S; (2016) Introduction to the radiation chemistry of polymers. In: Al-Assaf S, Coqueret X, Khairul Zaman HMD, Sen M, Ulanski P (eds.), The Radiation Chemistry of Polysaccharides, IAEA, Vienna, 25-76.

[46] Veith M, Moh K, Cavelius C; (2012) Synthesis of monodisperse silver nanoparticles by sonolysis of silver carboxylates. Advanced Engineering Materials 14(9), 825–829. **DOI:** 10.1002/adem.201200111

[47] Yeshchenko OA, Dmitruk IM, Alexeenko AA, Kotko AV, Verdal J, Pinchuk AO; (2012) Size and temperature effects on the surface plasmon resonance in silver nanoparticles. Plasmonics 7(4), 685–694. **DOI:** 10.1007/s11468-012-9359-z

[48] Car J, Krstulović N; (2022) Analytical model for determination of size-distribution of colloidal silver nanoparticles from surface plasmon resonance wavelength and dielectric functions. Nanomaterials 12(19), 3474. **DOI:** 10.3390/nano12193474

[49] Chen M, Luo S, Xu W, Zhang X; (2010) Ultrasonic synthesis of nano-size silver particles colloidal sol and its characterizations. Nano Science and Nano Technology An Indian Journal 4(1), 6–10.

[50] Pansara C, Mishra R, Mehta T, Parikh A, Garg S; (2020) Formulation of chitosan stabilized silver nanoparticle-containing wound healing film: in vitro and in vivo characterization. Journal of Pharmaceutical Sciences 109(7), 2196–2205. **DOI:** 10.1016/j.xphs.2020.03.028

[51] Oryan A, Alemzadeh E, Tashkhourian J, Nami Ana SF; (2018) Topical delivery of chitosan-capped silver nanoparticles speeds up healing in burn wounds: A preclinical study. Carbohydrate Polymers 200, 82–92. **DOI:** 10.1016/ j.carbpol.2018.07.077

[52] Shehabeldine AM, Salem SS, Ali OM, Abd-Elsalam KA, Elkady FM, Hashem AH; (2022) Multifunctional silver nanoparticles based on chitosan: antibacterial, antibiofilm, antifungal, antioxidant, and wound-healing activities. Journal of Fungi 8(6), 612. **DOI:** 10.3390/jof8060612

[53] Vanti G, Poondla N, Manogaran P, Teradal N, Veeresh S, Kaulgud R, Kurjogi M; (2024) Synthesis and characterization of multifunctional chitosan–silver nanoparticles: an in-vitro approach for biomedical applications. Pharmaceuticals 17(9), 1229. **DOI:** 10.3390/ph17091229

[54] Łosiewicz B, Osak P, Nowińska D; (2024) Recent advances in the electrophoretic deposition of chitosan-silver nanocomposite coatings on metallic implants with enhanced biocidal properties. Progress on Chemistry and Application of Chitin and its Derivatives 29, 7–20. **DOI:** 10.15259/PCACD.29.001

© Polish Chitin Society

Open Access: This article is distributed under the terms of the Creative Commons Attribution 4.0 International License (CC BY 4.0), which permits use, sharing, adaptation, distribution and reproduction in any medium or format, provided that appropriate credit is given to the original author(s) and source, a link to the license is provided, and any changes are indicated. Third-party material is included under the same license unless otherwise stated in a credit line.